The Astrophysical Journal, 473:1067–1078, 1996 December 20

SURFACE TEMPERATURE OF A MAGNETIZED NEUTRON STAR AND INTERPRETATION OF THE *ROSAT* DATA. II.

Dany Page and A. Sarmiento
Instituto de Astronomía, Universidad Nacional Autónoma de México, Apdo. Postal 70-264, 04510 México D.F., Mexico
Received 1996 February 7; accepted 1996 June 17

ABSTRACT

We complete our study of pulsars' nonuniform surface temperature and its effects on their soft X-ray thermal emission. Our previous work showed that, because of the effect of gravitational lensing, dipolar fields cannot reproduce the strong pulsations observed in the four nearby pulsars for which surface thermal radiation has been detected: PSR 0833−45 (Vela), PSR 0656+14, PSR 0630+178 (Geminga), and PSR 1055−52. Assuming a standard neutron star mass of 1.4 $M_\odot$, we show here that the inclusion of a quadrupolar component, if it is suitably oriented, is sufficient to increase substantially the pulsed fraction, PF, up to or above the observed values if the stellar radius is 13 km or even 10 km. For models with a radius of 7 km, the maximum pulsed fraction obtainable with (isotropic) blackbody emission is of the order of 15% for orthogonal rotators (Vela, Geminga, and PSR 1055−52) and only 5% for an inclined rotator such as PSR 0656+14. Given the observed values, this may indicate that the neutron stars in Geminga and PSR 0656+14 have radii significantly larger than 7 km, and given that very specific quadrupolar components are required to reproduce the large observed PF, even radii of the order of 10 km may be unlikely in all four cases. However, effects not included in our study might seriously invalidate this tentative conclusion.

We confirm our previous finding that the pulsed fraction always increases with photon energy, up to ∼1 keV, when blackbody emission is used, and we show that this is due to the hardening of the blackbody spectrum with increasing temperature. The observed decrease of the pulsed fraction may thus suggest that the emitted spectrum is softer in the warmest regions than in colder ones and that this observed effect must be of magnetospheric origin, probably due to the magnetic field.

Finally, we apply our model to reassess the magnetic field's effect on the outer boundary condition used in neutron star cooling models and show that, in contradistinction to several previous claims, it is a small effect.

Subject headings: pulsars: general — stars: magnetic fields — stars: neutron — X-rays: stars

1. INTRODUCTION

In a previous paper (Page 1995a, hereafter Paper I), we presented a simple but realistic model of temperature distribution at the surface of a magnetized neutron star. This model was used to study the effects of temperature inhomogeneity on neutron star thermal emission and compare them with the observed properties of the four neutron stars for which this emission has been detected by *ROSAT* (Ögelman 1995; Page 1995b): PSR 0833−45 (Vela; Ögelman, Finley, & Zimmermann 1993), PSR 0656+14 (Finley, Ögelman, & Kiziloğlu 1992), PSR 0630+178 (Geminga; Halpern & Holt 1992), and PSR 1055−52 (Ögelman & Finley 1993). As a first step, we did not take into account magnetic effects in the atmosphere, which are also very large. We also restricted ourselves to dipolar magnetic fields, and the main results we obtained were the following:

1. Magnetic effects on heat transport in the neutron star's envelope do induce very large temperature differences at the surface, but when gravitational lensing is taken into account and only dipolar fields are considered, the predicted pulsed fractions are smaller than those observed in the soft band, where the surface thermal emission is seen. In particular, in the case of 1.4 $M_\odot$ neutron stars with small radii, ∼7.0–9.0 km, the pulsed fractions, PF, are below 1%. With very small radii, ≤6.5 km, and the same mass, gravitational beaming can however increase PF up to 6%–7%. Observed values of PF range between 10% and 30%.

2. With dipolar fields, the observable light curves are very symmetric, and their shapes do not correspond to the observations. Together with the previous result, this led us to conclude that the inclusion of only dipolar fields is not adequate to model the surface magnetic field of the four observed neutron stars.

3. The amplitude of the pulse profile increases with increasing photon energy. This result does not correspond to what is observed in the soft X-ray band in the case of Geminga and also, but to a lower degree, in PSRs 0656+14 and 1055−52.

Here we complete this study and consider also the effects of these surface temperature distributions on the cooling of neutron stars. Since the completion of the work presented in Paper I, complementary results considering the magnetic effects in the atmosphere, where the emerging spectrum is generated, have been presented (Pavlov et al. 1994; Zavlin et al. 1995) and clearly shown that they can be as important as the magnetic effects in the envelope that we consider here and in Paper I. A complete study must obviously include both aspects of the problem, envelope and atmosphere. However, as long as the exact chemical composition of a pulsar's surface is not known, analysis with blackbody (BB) emission will still remain a mandatory first step and a reference to which atmospheric models will be compared. For this reason it is important to characterize BB emission and determine what can and what cannot be obtained with it. As important as the successes of our model will thus be its failures, which can guide us toward the correct atmospheric, or more generally surface, model (Page 1995b; Page, Shibanov, & Zavlin 1995). Nevertheless, several of our results are, we hope, sufficiently general and robust to be valid despite the limitations of BB emission. We restrict ourselves to studying general properties of the model and refrain from detailed analyses of the data, which we leave for future work. Our method to generate surface temperature distributions and the observable X-ray fluxes is described in detail in Paper I.

Our basic results are in § 3, where we consider the effects of the inclusion of the quadrupolar components of the magnetic field and show that, when they are superposed on a dipolar field, they provide a sufficiently general configuration for our study. The following sections are mostly applications of the results of § 3 and are only loosely related to each other. Beforehand, in § 2, we present some complements to our summary of the *ROSAT* data given in Paper I. Some basic and straightforward results are presented in §§ 4 and 5. We use the dipole-plus-quadrupole configurations to discuss the possibility of putting constraints on the neutron star size through gravitational lensing in § 6. We then discuss the energy dependence of the light curves' amplitude in § 7; this section will give a clear indication of the inadequacy of BB emission for understanding detailed features of the observations. The next section, § 8, adds a second component of emission in order to model the higher energy tail of Geminga. Section 9 studies the effect of the surface temperature distribution on the boundary condition used for modeling the thermal evolution of neutron stars. Finally, § 10 presents our conclusions.

2. THE *ROSAT* DATA

Since the completion of Paper I, some information has been presented on the second set of *ROSAT* observations of PSR 0656+14 (Ögelman 1995; Possenti, Mereghetti, & Colpi 1996). The complete set of data clearly shows the presence of a hard tail that is strongly pulsed, as in Geminga and PSR 1055−52. The energy dependences of both the pulsed fraction and the pulse phase show some similarity with PSR 1055−52 (Ögelman 1995) and also with Geminga (H. Ögelman 1995, private communication): in all three cases, PF is almost constant up to channel ~ 40 (~ 30 for Geminga), then decreases and finally increases (very strongly in the case of PSR 1055−52). Moreover, at around the same energy at which PF increases, the phase of the peak changes. The spectral fits with a soft BB for the surface thermal emission and a BB or power law for the hard tail show that the surface thermal emission dominates below channel ~ 50 in the case of Geminga (e.g., Fig. 5 below) and channel ~ 100 in the cases of PSR 0656+14 and PSR 1055−52 (see, e.g., Ögelman 1995). An important point is that, in the case of Geminga, the change in the peak phase and the increase of PF coincide with the spectral shift from the surface thermal emission to the hard tail (see § 8) and are not surprising. However, in the two other cases, this phase shift apparently, and intriguingly, occurs within the band dominated by the surface thermal emission.

3. DIPOLE-PLUS-QUADRUPOLE FIELDS

Since we have shown in Paper I that purely dipolar surface magnetic fields are not sufficient to interpret the *ROSAT* data, the next natural step is the inclusion of a possible quadrupolar component. We make precise in the Appendix our notation and also describe the effect of gravity on the magnetic field, which is not as important as redshift and lensing but is nonetheless not completely negligible, since it can substantially increase the field strength, and is moreover straightforward to implement.

Since the quadrupolar components introduce five more degrees of freedom, a clear general assessment of their possible effects is necessary. To investigate this, we computed nine sets of 1000 models each, in which the quadrupolar components were chosen at random by the computer; three orientations of the dipole and observer, $\alpha = \zeta = 30°$, $60°$, and $90°$, were taken to test for geometric effects (α is the angle between the rotation axis and the dipole and ζ is the angle between the rotation axis and the observer's direction), and three values for the stellar radius, $R = 7$, 10, and 13 km, were used to analyze the effect of gravitational lensing. The maximum lensing angles, $\theta_{\max}$, are 194°, 132°, and 117° for radii of 7, 10, and 13 km, respectively (see Fig. 3 in Paper I). The dipole strength was fixed at 10^{12} G (the value at the magnetic pole in flat spacetime; general relativistic effects increase it slightly), and the 1000 quadrupoles were added to the basic dipole. The quadrupole component strengths, Q_i, were restricted to the range 10^{10}–(5×10^{12}) G. The star's surface temperature was calculated using an interior temperature of $T_b = 10^8$ K, which implies an effective temperature around 10^6 K (the exact value depending on the star size and field configuration). Note that general relativistic effects depend only on the ratio $R/R_S = Rc^2/2GM$ of the star's radius R to its Schwarzschild radius R_S, so all our results can be extrapolated to other masses and radii (see, e.g., Fig. 8 below for easy conversion). To save CPU time, we only calculated the variation of the observable phase-dependent effective temperature, T_e^{Φ} (Paper I, § 5.2), during the star's rotation, i.e., the effective temperature of the portion of the stellar surface visible to the observer at a given phase Φ. Selecting a subset of the 9000 models so generated, we performed complete calculations of the detectable fluxes to calibrate the observable pulsed fraction PF, in the *ROSAT* Position Sensitive Proportional Counter (PSPC) channel range 7–50, in terms of the pulsation of T_e^{Φ}. The results of these calculations are shown in Figure 1, where each model is shown as a dot and the pure-dipole case as a black-and-white ring. The dramatic effect of lensing is again clearly seen. For later use, Figure 1 plots the ratio of the star's effective temperature $T_e(\mathrm{D+Q})$ for the given dipole-plus-quadrupole field configuration to the effective temperature with only the dipolar field, $T_e(\mathrm{D})$. A different T_b would change the values of PF but not significantly change the statistics. The observable PF increases with decreasing temperature for a given surface magnetic field configuration, as explained in § 4.

We want here to correct our definition of the pulsed fraction (eq. [21] in Paper I) and rather use its standard expression as the fraction of counts above minimum; thus

$$\mathrm{PF}(i) = \frac{\mathrm{Cts}_{\mathrm{mean}} - \mathrm{Cts}_{\mathrm{min}}}{\mathrm{Cts}_{\mathrm{mean}}}, \tag{1}$$

where $\mathrm{Cts}_{\mathrm{mean}}$ and $\mathrm{Cts}_{\mathrm{min}}$ are, respectively, the mean and minimum count rates detected during the star's rotation in channel i. For sinusoidal pulse profiles, or low values of PF, this is equivalent to our former definition and does not affect the results of Paper I.

The first obvious and natural result of Figure 1 is that most configurations produce little pulsation: most quadru-

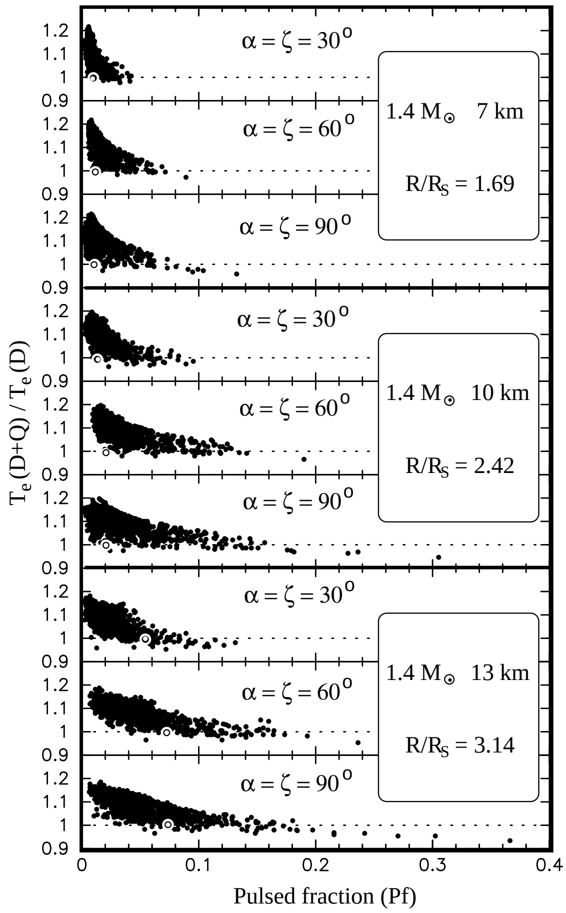

FIG. 1.—Statistics of observable pulsations with dipole-plus-quadrupole magnetic fields. For each stellar radius and dipole-observer orientation (α-ζ) with respect to the rotational axis, 1000 dipole-plus-quadrupole surface magnetic fields and the induced temperature distribution were generated. The x-axis plots the observable pulsed fraction in the PSPC channel band 7–50 for the given surface temperature distribution, and the y-axis plots the ratio of the star's effective temperature for the given dipole-plus-quadrupole magnetic field configuration, T_e(D + Q), to the effective temperature of the pure-dipole case, T_e(D). The surface temperatures are calculated from an interior temperature $T_b = 10^8$ K; all models have an effective temperature around 10^6 K. Lowering T_e does increase PF, by $\sim 15\%$ at $T_e \sim 3 \times 10^5$ K and 30% at 10^5 K. See § 3 for more details.

poles induce several warm regions, which flatten the pulse profile even below the value of the pure-dipole case. However, many configurations do increase PF substantially, compared to the pure-dipole case, and to a high value in some special cases. We can thus obtain observable pulsed fractions higher than 30% (at energies below 0.5 keV and at $T_e \sim 10^6$ K) for a star of radius 13 km. For stars of radii 10 km, a PF value comparable to those observed can also be obtained. In the case of a 7 km radius star, despite the enormous gravitational lensing ($\theta_{\max} = 194°$), we could still find one configuration that yields a PF above 10% at high T_e ($\sim 10^6$ K) and above 15% at $T_e \sim 3 \times 10^5$ K, as we have checked explicitly.

A last point is worth mentioning: the strong increase in the pulsed fraction possible with the addition of a quadrupolar component is *not* due to a large increase in the area of the cold regions, compared to the pure-dipole case, but rather to a displacement of the magnetic poles and the surrounding warm regions that brings them closer to each other (see, e.g., Fig. 2). Since the ratio T_e(D + Q)/T_e(D) is slightly lower than unity for the highly pulsed models, there is however a slight relative increase of the cold regions.

The pulse profiles of Geminga and PSR 1055 − 52, which are both considered to be almost orthogonal rotators, show a single wide peak, which indicates that the two polar caps and the surrounding warm regions are much less than 180° apart. How close the magnetic poles can be pushed toward each other is what will determine the "success" of the quadrupolar component in increasing the pulsed fraction, whereas quadrupoles that moreover introduce several new warm regions will fail. Figure 1 illustrates this clearly: T_e(D + Q)/T_e(D) is only slightly below 1 for the strongly pulsed dipole-plus-quadrupole configurations while weakly pulsed configurations that induce several warm regions may have a ratio larger than 1. These considerations will be of importance in § 9.

4. EFFECT OF THE FIELD STRENGTH AND RELIABILITY OF THE TEMPERATURE MODEL

Considering the effect of the field strength, in the pure-dipole case we found that the maximum PF is obtained when the overall surface field reaches a few times 10^{11} G (Paper I); the same result still applies to the dipole-plus-quadrupole case. Below (2–3) $\times 10^{11}$ G, the magnetic effects are becoming smaller, and above this value, even if the magnetic effects are increasing, the resulting observable PF varies very little. The reason the pulsed fraction depends very weakly on the field strength for large enough fields is simple: cold regions contribute so little to the total flux that it does not really matter how cold they are (as determined by the field strength), but only how large they are (determined by the field geometry).

We are thus dealing mostly with warm plates whose extension is determined more by the field orientation than by the field strength as long as the field strength does not drop below a few times 10^{11} G. The simple formula (Greenstein & Hartke 1983) for the temperature T_s at a given point on the neutron star's surface,

$$T_s(g_s, T_b; B, \Theta_B) = T_{s\parallel}(g_s, T_b; B)(\cos^2 \Theta_B + \chi_0^4 \sin^2 \Theta_B)^{1/4} \tag{2}$$

(with g_s the surface gravitational acceleration, T_b the internal temperature, B the magnetic field strength at the point considered and Θ_B its angle with the surface's normal,

$$\chi_0 \equiv T_{s\perp}(g_s, T_b; B)/T_{s\parallel}(g_s, T_b; B)\,, \tag{3}$$

and $T_{s\perp}$ [resp., $T_{s\parallel}$] is the temperature the surface would have if Θ_B were 90° [resp., 0°]; see Paper I and Shibanov & Yakovlev 1996), which we use to define the surface temperature distribution (Paper I), can be simplified for a large enough field (above $\sim 3 \times 10^{11}$ G, since then $\chi_0^4 \ll 1$) to

$$T_s(\Theta_B) = T_{s\parallel} \cos^{1/2} \Theta_B \tag{4}$$

to a good approximation as long as Θ_B is not too close to 90°. So the dependence of $T_s(\Theta_B)$ on $T_{s\perp}$ practically drops out, except when $\Theta_B \sim 90°$, but then T_s is so low that the region makes a negligible contribution to the total stellar flux. This is fortunate since $T_{s\perp}$ is poorly known (see discussion in Paper I and Page 1995b) and shows that our model of temperature distribution is reliable for present practical purposes.

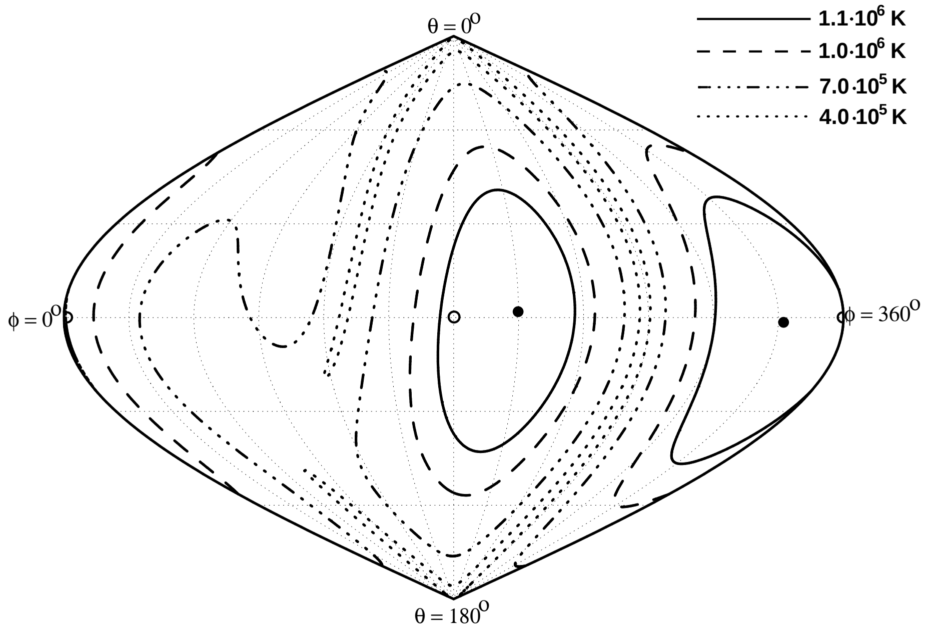

FIG. 2.—Surface temperature distribution for the dipole-plus-quadrupole magnetic field configuration of Fig. 1 that yields the highest observable pulsed fraction. The whole star's surface is shown in an area-preserving mapping. With an internal temperature of 10^8 K, the effective temperature is 9.33×10^5 K while the maximum and minimum temperatures are, respectively, 1.2×10^6 and 3.1×10^5 K (1.4 $M_\odot$ star with a 10 km radius). Four sets of isotherms are plotted, as indicated. The field components consist of a dipolar component of strength 10^{12} G and orientation $\theta = 90°$ and $\phi = 0°$, and quadrupolar components of strengths $Q_0 = 2.48 \times 10^{10}$ G, $Q_1 = 6.84 \times 10^{10}$ G, $Q_2 = 5.01 \times 10^{10}$ G, $Q_3 = 4.80 \times 10^{11}$ G, and $Q_4 = -6.24 \times 10^{10}$ G; the maximum field strength at the surface is 2.18×10^{12} G, and the minimum is 1.72×10^{11} G. The two filled circles show the approximate locations of the polar caps, obtained by integrating the last open magnetic field lines from the light cylinder down to the stellar surface, while the two open circles at $\theta = 90°$ and $\phi = 180°$ and 360° show their positions without the quadrupolar component.

5. EFFECT OF THE TEMPERATURE DISTRIBUTION ON THE SPECTRUM

The surface temperature distributions induced by dipole-plus-quadrupole fields can have quite complicated structures. However, as discussed in Paper I for dipolar fields, the resulting phase-integrated spectra are close to single-temperature spectra at the corresponding effective temperature. Figure 3 shows examples at five temperatures for the dipole-plus-quadrupole field from the set generated for Figure 1 (see § 3) that yields the highest pulsed fraction. The surface temperature distribution induced by this field configuration is illustrated in Figure 2. The result is very close to the effect of a simple dipole (see Fig. 6 in Paper I) because the chosen quadrupole induces warm regions of approximately the same size as the pure dipole, but at different locations (see § 3). When taking into account the PSPC's response (Fig. 3*b*), the composite spectrum presents a clear excess compared to the single-temperature spectrum at channels above 40–60. This excess will not affect spectral fits in the case of Geminga since the flux at channels above 60 is dominated by the hard tail. However, in the three other cases, in which the hard tail only appears above 1 keV, even above 1.2 keV for Vela, this excess will have some impact on the temperature measurement: spectral fits with

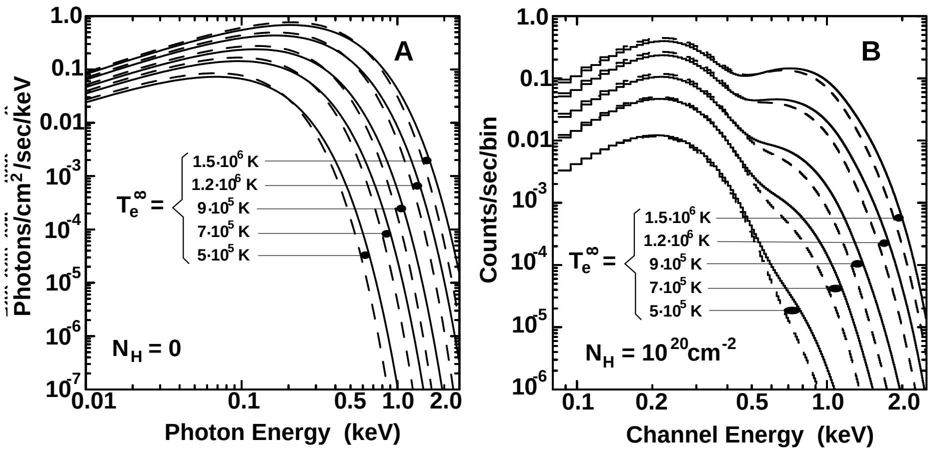

FIG. 3.—Effect of the inhomogeneous surface temperature on the spectrum. *Left*, incident flux (i.e., with redshift and lensing) at five temperatures, with zero interstellar absorption; *right*, the same fluxes with interstellar absorption and passed through the PSPC's response matrix. The temperatures of 5, 7, 9, and 15×10^5 K correspond to the estimated blackbody temperatures of Geminga, PSR 1055−52, PSR 0656+14, and Vela, respectively. We used a 1.4$M_\odot$, 10 km radius ($R^\infty = 13.06$ km) star, at a distance of 500 pc, with the same field configuration as in Fig. 2. Solid curves show composite BB spectra, dashed curves single-temperature BB spectra at $T = T_e$.

composite BB spectra may yield slightly lower values of T_e^∞ than single-BB spectra and may require slightly lower N_H-values. This is also valid with purely dipolar fields since they induce warm and cold regions of area similar to the strongly pulsed dipole-plus-quadrupole configurations considered here. However, Possenti et al. (1996) estimate, in the case of PSR 0656+14 with a dipolar field, that this does not affect the spectral fits, as a result of the present observational limitations. We will not attempt to quantify this small effect here since we restrict ourselves to general characteristics of our model. This excess in the Wien tail may also affect parameter values for the fits of the hard tail for PSRs 0656+14 and 1055−52, but in the case of Geminga our illustrative fit of § 8 can be performed with the same parameter as used by Halpern & Ruderman (1993) for uniform surface temperature.

6. GRAVITATIONAL LENSING AND NEUTRON STAR SIZE

It was shown in Paper I that, because of gravitational lensing, when only dipolar fields are used the pulsed fraction PF obtained is lower than what has been detected. The addition of a quadrupolar component can substantially increase PF, to values comparable to those observed, as shown in § 3 (Fig. 1). However, for this to happen, we must choose carefully the strengths of the several $\boldsymbol{b}_i$ compared to the dipole's strength and orientation: random quadrupolar components generally yield temperature distributions that are so complicated that they flatten the light curves.

Vela and PSR 1055−52 have pulsed fractions slightly higher than 10% in the channel band in which surface thermal emission is detected, and they are considered to be almost orthogonal rotators; the models of Figure 1 with $\alpha \sim \zeta = 90°$ thus apply to them. Taking into account that the effective temperature of PSR 1055−52 is lower than 10^6 K, the observable PFs would be slightly higher than the values shown in Figure 1. We see that, for 1.4 $M_\odot$ stars with radii of 13 or 10 km, many models can produce PFs as high as observed. However, only a very few, special field configurations can reproduce the observed PF at $R = 7$ km, less than 0.1% of all configurations generated randomly for Figure 1. The high PF $\sim$ 20%–30% of Geminga, also an orthogonal rotator, is however not reproducible with a 7 km radius 1.4 $M_\odot$ star (i.e., with $R = 1.7R_S$): the most strongly pulsed dipole-plus-quadrupole model that we found yields, at $T_e = 5 \times 10^5$ K, a fraction PF $\sim$ 15% in channel band 7–50, as we have checked explicitly, and only a few models at 10 km radius reach 20% modulation. In the case of PSR 0656+14, which has a BB effective temperature of $\sim 8 \times 10^5$ K and $\alpha \sim \zeta \sim 30°$, we can obtain the observed PF $\sim$ 14% with a 13 km radius 1.4 $M_\odot$ star with many models and at 10 km radius in only a few cases, but with no model at all for a 7 km star; in this latter case, the highest PF we can obtain is $\sim$4%. If we take $\alpha \sim \zeta \sim 8°$ (Lyne & Manchester 1988), then PF is always extremely small: even with a radius of 13 km, for a mass of 1.4 $M_\odot$, the same procedure as used for Figure 1 could not find any model (out of 1000) that yields a PF higher than 4%.

7. ENERGY AND TEMPERATURE DEPENDENCE OF THE PULSED FRACTION

One of the most important characteristics of the observed pulsations is the energy dependence of the pulsed fraction, PF. We showed in Paper I that BB emission with dipolar fields always produces an *increase* of PF with photon energy. We confirm this here, with a few exceptions, for more general temperature distributions and explain the origin of this feature.

The reason for the increase of PF with energy for BB emission was elucidated by Page et al. (1995): the hardness of the BB spectrum *increases* with energy. The ratio of the BB fluxes emitted at energy E by two regions of areas A_1 and A_2 with respective temperatures T_1 and T_2 is

$$\frac{F_{\rm BB}(E,\, T_1)}{F_{\rm BB}(E,\, T_2)} = \frac{A_1}{A_2}\,\frac{\exp\,(E/k_{\rm B}T_2) - 1}{\exp\,(E/k_{\rm B}T_1) - 1}\,, \tag{5}$$

which is an *increasing* function of E if $T_1 > T_2$. This means that if we have a warm spot at temperature T_1 on a surface with uniform temperature $T_2 < T_1$, then PF naturally increases with energy. A smooth temperature distribution with only one peak in temperature will obviously yield the same result. We can state by experience that, with several peaks, PF always increases (with increasing channel energy) up to channel $\sim$60 for $T_e \sim 5 \times 10^5$ K and up to channel $\sim$100 for $T_e \sim 10^6$ K—we have tried *many* models with dipoles, off-centered dipoles, quadrupoles, dipoles plus quadrupoles, warm plates, and found no exception. Only in a few special cases have we " observed " a decrease in PF in the Wien tail, which is due to the following (Fig. 4): The surface presents two warm regions on opposite sides of the star, a very large one and a smaller one where the temperature reaches a slightly higher value (Fig. 4*a*), and only one peak is visible, i.e., the peak from the small, warmer region does not appear as a peak but is only filling the dip between the successive peaks of the large region (Fig. 4*b*). By looking at increasing energy, the filling of the small peak increases (the small region is warmer than the large one), and PF thus decreases (Fig. 4*c*). If the area of the small, warmer region is increased, then it produces a distinct peak, i.e., we obtain a double-peaked light curve, the amplitude of both peaks increases with energy (the amplitude of the small-region peak will eventually win over the large-region one), and PF increases. It thus seems that the only mechanism, with BB emission, that can produce a decrease in PF is this filling of the interpeak region by emission from a small, slightly warmer region. This is in fact the mechanism that Halpern & Ruderman (1993) invoked to explain the observed decrease of PF (in channels 28–53 vs. 7–28) in Geminga, but with an essential difference: they proposed that the hard-tail component, which is $\sim$100° out of phase with the thermal component, would fill the dip in the light curve. However, the hard tail is much harder than the surface thermal component, i.e., clearly separable from it in the spectrum, and cannot actually produce a decrease in PF at energies below 0.5 keV, as we show in the next section. In the cases in which we have " observed " a decrease in PF, the component responsible is only slightly warmer than the rest of the star, and its emission is practically indistinguishable in the spectrum.

Another feature encountered in Paper I, for dipolar fields, was a steepening of the increase of PF in the channel band 50–70, which is due to the response of the PSPC: we see that this effect is still present with dipole-plus-quadrupole fields and will be general for all spectra that produce an increase in PF at energies around 0.5 keV (see, e.g., Figs. 4*c* and 5*c*).

For a given field configuration, the observable PF at a given energy increases when the overall stellar effective tem-

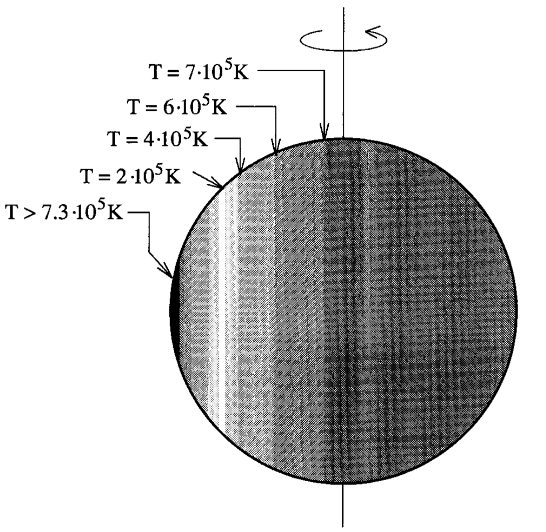

FIG. 4*a*

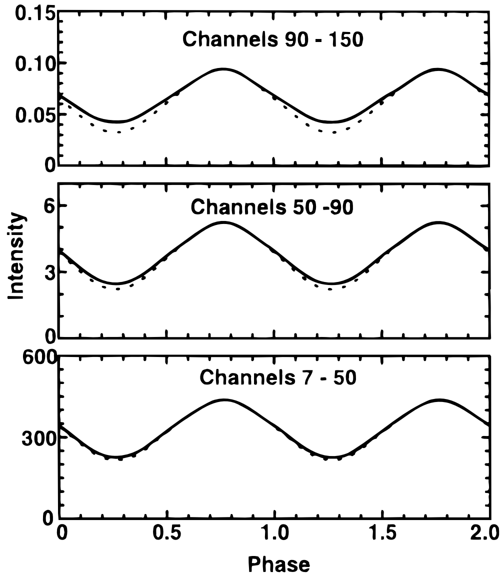

FIG. 4*b*

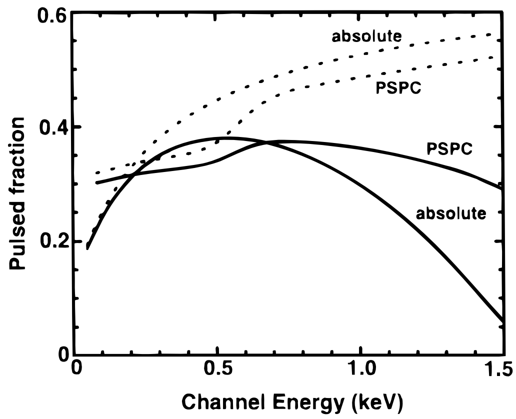

FIG. 4*c*

FIG. 4.—A model that produces a decreasing pulsed fraction with blackbody emission. (1.4 $M_\odot$ star with a 12 km radius.) (*a*) Surface temperature distribution. The magnetic field is a dipole orthogonal to the rotation axis (in direction $\theta = 90°$ and $\phi = 0°$) with its center shifted by a half-radius in the direction of the north magnetic pole. The warm region around the north pole reaches a temperature of 8.15×10^5 K but is much smaller than the warm region around the south pole, whose maximum temperature is 7.25×10^5 K. (*b*) Light curves in three channel bands produced by the temperature distribution of (*a*), as seen through the *ROSAT* PSPC by an observer at 150 pc and $N_H = 10^{20}$ cm^{-2}. The star's rotation axis is along $\theta = 0°$ and the observer is at $\theta = 90°$. The dotted lines show light curves for which the temperature of the smaller north magnetic pole region has been blocked at 7.25×10^5 K, i.e., the same maximum temperature as the large region around the south magnetic pole; this clearly shows that this warmest region is responsible for the decrease of the PF. (*c*) Observable (with the PSPC) and absolute (i.e., as would be seen with a perfect energy resolution detector) PFs. The dotted curves show the corresponding PF when the temperature of the small, warm region has been blocked at 7.25×10^5 K, as in (*b*).

perature decreases. We stated, wrongly, in Paper I that this was due to the increase of the temperature difference between the warm and cold regions when T_b decreases. However, a much stronger temperature-difference increase is induced by the increase of the field strength, and it has almost no effect on PF, as stated in § 4. The actual reason for the increase of PF at a given energy with decreasing T_e is the decrease of PF with photon energy, since lowering T_e pushes the Rayleigh-Jeans part of the spectrum (which has a lower PF) out of the PSPC range and brings in the more strongly pulsed, higher part of the spectrum.

8. SEPARATION OF THE SURFACE THERMAL EMISSION FROM THE HIGH-ENERGY TAIL

Our study so far, and in Paper I, has concentrated exclusively on the soft X-ray band, assuming implicitly that this thermal component can be separated from the hard tail. We argue here that this separation is justified and show it explicitly for the case of Geminga. A simple look at the spectral fits (e.g., Fig. 5*a* below, or Halpern & Ruderman 1993 for Geminga; Ögelman 1995 for PSRs 0656+14 and 1055−42) shows that, at energies slightly below the crossover of the soft thermal component with the hard tail, the contribution of the latter rapidly becomes negligible compared to the former. Moreover, the spectral fit of the soft component is not changed significantly whether the hard tail is fitted by BB emission or power-law emission (see, e.g., Halpern & Ruderman 1993). We thus do not expect much interference between these two components.

The contribution of the hard tail to the soft band is larger if it is modeled as a power law rather than a BB. To consider the worst case of interference between the two spectral components, we thus model Geminga's X-rays with a composite model including surface thermal emission and a pulsed power-law tail, the results being shown in Figure 5. The same surface temperature model complemented with a

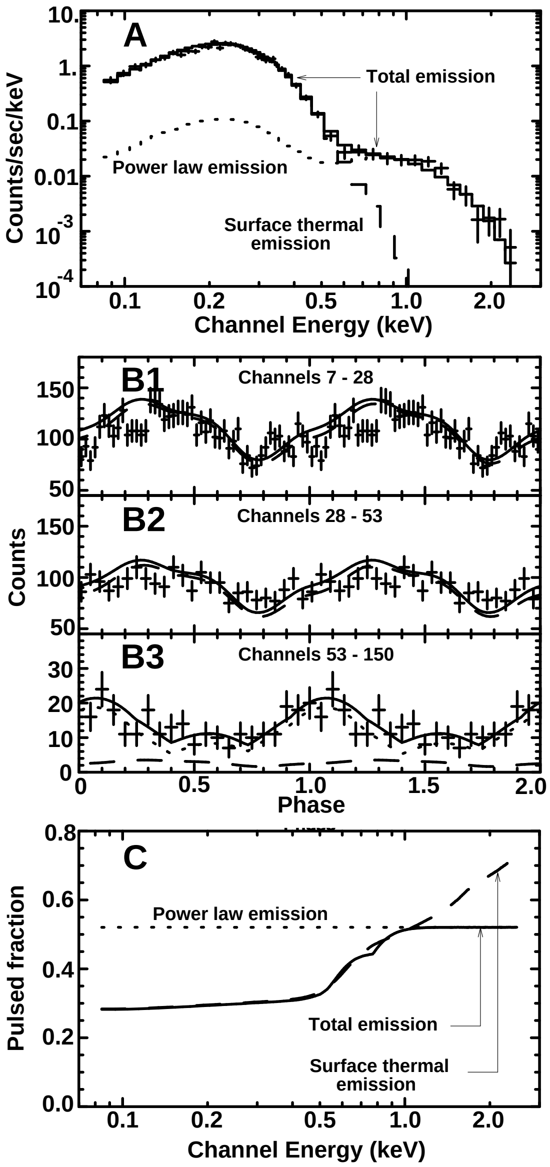

FIG. 5.—Composite model of Geminga's soft X-ray emission: surface thermal emission (*dashed lines*) plus power-law emission (*dotted lines*) and total emission (*solid lines*). Surface temperature distribution induced by a dipole-plus-quadrupole magnetic field: a dipole of strength 10^{12} G perpendicular to the rotational axis and a quadrupole with components $Q_0 = -2.28 \times 10^{11}$ G, $Q_1 = +4.95 \times 10^{10}$ G, $Q_2 = +3.36 \times 10^{10}$ G, $Q_3 = +7.08 \times 10^{11}$ G, and $Q_4 = -4.53 \times 10^{11}$ G. The interior temperature is 4.04×10^7 K, yielding an effective temperature at infinity $T_e^\infty = 4.30 \times 10^5$ K for a 1.4 $M_\odot$ star with radius of 12 km. The hard tail is a sum of two components, both power laws with index 1.47, modulated with the rotational phase Φ by a cos Φ factor. The observer is located within the rotational equatorial plane at a distance of 185 pc, and $N_H = 2.1 \times 10^{20}$ cm^{-2}. (*a*) Observable count rates from the surface thermal emission, the power-law emission, and the total emission compared with the *ROSAT* data (from Halpern & Ruderman 1993). (*b*) Pulse profiles in three channel bands, compared with the *ROSAT* data (from Halpern & Ruderman 1993). (*c*) Pulsed fraction for the two components and the total emission.

hard tail as thermal emission from two polar caps has been presented in Page & Sarmiento (1996). The spectrum (Fig. 5*a*) shows that the hard-tail emission is ~ 30 times weaker than the surface emission below channel 40, but because of its strong pulsations, its contribution to the pulse profiles can be ~ 10% in the soft band, channels 7–28 (Fig. 5*b*; *top*). Nevertheless, this is far from enough to alter the shape of the light curves in both bands 7–28 and 28–53 (Fig. 5*b*; *middle*, *bottom*). The important consequence of this is the effect on the energy dependence of the pulsed fraction, shown in Figure 5*c*: the general trend typical of BB emission, consisting of an increase of PF with energy (see § 7), is slightly weakened by the addition of the hard tail but not reversed at channels below 100 (Fig. 5*c*). When modeled as polar-cap thermal emission, the hard tail's contribution to the soft band is almost completely negligible (Page & Sarmiento 1996). It is thus not possible, within the present framework, to make the hard tail responsible for the observed decrease of the pulsed fraction with energy below 0.5 keV. The observed decrease of PF with energy at channels below 53 observed in Geminga is most certainly an intrinsic property of the surface thermal emission that is absolutely irreproducible with BB emission.

The cases of PSR 0656+14 and PSR 1055−52 are more delicate, but from a look at the spectral fits, there is no doubt that the observed decrease of PF at channels below 70 and 50, respectively (Ögelman 1995), is also a property of the surface thermal emission since the crossover with the hard tail occurs around channel 100 for these two pulsars. However, the shift in the peak phase (Ögelman 1995) that occurs within the band dominated by the surface thermal emission is another feature totally unexplainable with BB emission. Thus both the pulsed-fraction variation and the peak phase shift must be attributed to the anisotropy induced by the magnetic field in the atmosphere, i.e., anisotropy of the emitted flux, superposed on a nonuniform surface temperature distribution. In the case of Geminga, the shift in the peak phase coincides with the shift from the surface thermal emission to the hard tail (H. Ögelman 1995, private communication) and is not surprising.

9. SURFACE BOUNDARY CONDITION FOR NEUTRON STAR COOLING

A direct application of our surface temperature model and of the previous analysis concerns the modeling of neutron star thermal evolution. In such models, the relationship between the temperature at the bottom of the envelope, T_b, and at the stellar surface, T_s, is needed as an outer boundary condition. Taking into account the surface temperature inhomogeneity, we must speak of a T_b-T_e rather than a T_b-T_s relationship, where T_e is the effective temperature of the whole surface, and, given different field structures, we can easily generate many such T_b-T_e relationships. Cooling models that include magnetic effects in the envelope have been presented by Van Riper (1991) and Haensel & Gnedin (1994), who used a radial-field T_b-T_e relationship; this is not a realistic configuration, and we will show here that a more careful treatment may actually lead to conclusions opposite to that reached by these authors. For a radial field, T_e is increased compared to the nonmagnetic case at a fixed T_b, as shown in Figure 1 of Paper I; during the photon-cooling era, i.e., neutron star age above $\sim 10^5$ yr, this results in an increased surface photon emission for a given internal temperature T_b and accelerated cooling compared to the nonmagnetic case. For example, with a radial field of strength 10^{13} G, T_e is increased by ~ 25% compared to the nonmagnetic case, and thus the photon luminosity is increased by a factor of 2.5.

The minimal inclusion of the magnetic field in the T_b-T_e relationship should be done with a dipolar geometry. If we consider, in equation (2), χ_0 as a constant along the surface, which we call $\bar{\chi}$, and integrate it for a dipolar field

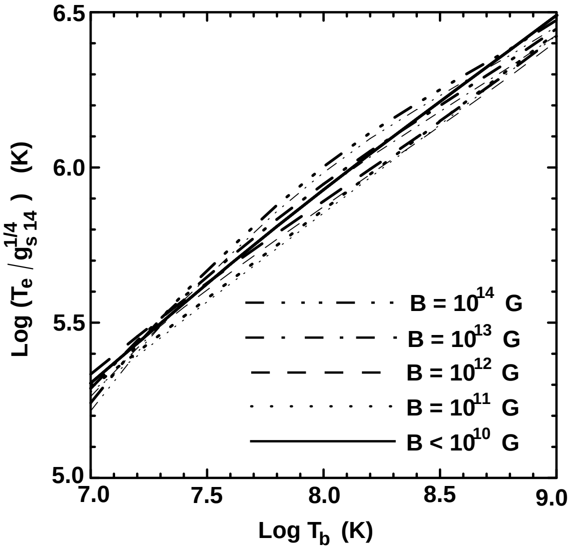

FIG. 6.—T_b-T_e relationship. Thick lines correspond to purely dipolar fields while the thin lines correspond to one of the maximally pulsed dipole-plus-quadrupole configurations of Fig. 1. The indicated field strengths are the dipole component strength at the magnetic pole (without general relativistic correction, so the actual field value is $\sim$50%–100% higher; see Fig. 8).

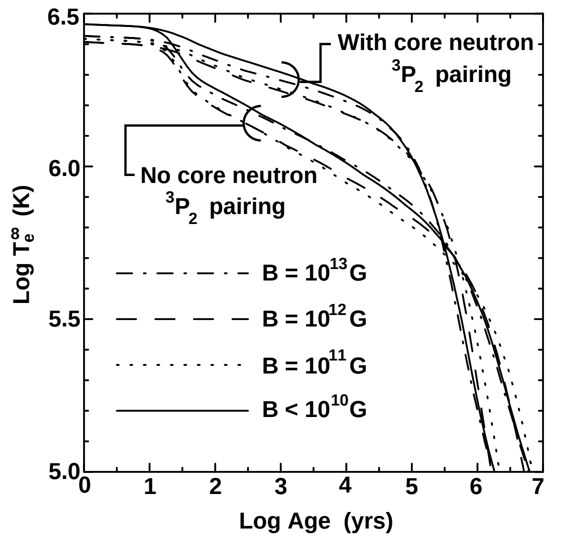

FIG. 7.—Effect of the crustal magnetic field on the cooling of neutron stars. We show the "standard" cooling of a 1.4 $M_\odot$ neutron star built with the Friedman & Pandharipande (1981) equation of state, both with and without core neutron $^3P_2$ pairing. The neutron core pairing critical temperature T_c is taken from Hoffberg et al. (1970); the high T_c of this calculation shows the maximum effect of pairing. Crustal neutrons are always assumed to be paired in the $^1S_0$ state, with T_c taken from Ainsworth, Wambach, & Pines (1989). Core neutron pairing has no effect at early stages ($\lesssim$20 yr) but (1) slows down cooling during the neutrino-cooling era (age up to $\sim 10^5$–10^6 yr) by strongly suppressing the neutrino emission and (2) hastens the cooling later, during the photon-cooling era, by suppressing the star's specific heat by $\sim$75% (see, e.g., Page 1994). The two sets of four curves show the effect of the crustal magnetic field on the cooling by its influence on the outer boundary condition. The four T_b-T_e relationships are taken from Fig. 6. During the neutrino-cooling era, the surface temperature follows the evolution of the core temperature: a T_b-T_e relationship that yields a higher T_e for a given T_b results naturally in a higher stellar effective temperature. During the subsequent photon-cooling era, the effect is inverted since the dominating energy loss is from surface thermal emission with luminosity $L_\gamma = 4\pi R^2 \sigma T_e^4 \sim T_b^2$ (using $T_e \propto T_b^{0.5}$ from Fig. 6), and a higher T_e for a given T_b results in a larger L_γ. Calculations were performed with the cooling code used by Page (1994).

(neglecting the gravitational corrections), we easily obtain

$$T_e(g_s, T_b) = T_{s\parallel}(g_s, T_p; B_p)[1 - 0.47(1 - \bar{\chi}^4)]^{1/4} \qquad (6)$$

for the effective temperature T_e as a function of the maximum surface temperature $T_{s\parallel}(g_s, T_b; B_p)$ near the magnetic poles (B_p being the field strength at the magnetic pole); this reduces the magnetic field's effects and brings the T_b-T_e relationship close to the nonmagnetic one (when $\bar{\chi} \ll 1$, the numeric factor in eq. [6] is $\sim$0.85). The exact integration (taking into account the field dependence of χ_0) can only be accomplished numerically and as is illustrated in Figure 6.

Since we have shown that the surface field of the four pulsars that show surface thermal emission (and can be compared with cooling models) is not dipolar, we must include the quadrupolar component in the T_b-T_e relationship. A general idea of the effect can be immediately seen from Figure 1, which shows T_e(D + Q)/T_e(D) (for a dipole strength of 10^{12} G). At $T_b = 10^8$ K, i.e., $T_e \sim 10^6$ K, most configurations result in a T_e higher than the pure-dipole case. However, T_e(D + Q)/T_e(D) decreases for configurations with larger PF and is systematically slightly smaller than 1 for the cases that can produce the large observed pulsed fractions. We also show, in Figure 6, a second T_b-T_e relationship that corresponds to the most strongly pulsed configuration that we have found with a dipole-plus-quadrupole field and shows the very slight reduction of T_e ($\sim$5%) compared to the dipole case. We have explicitly verified that other field configurations that produce large observable pulsations yield almost identical results, as can also be seen from Figure 1. The interesting result is that this relationship does not depend significantly on the field configuration (for strongly pulsed models) and is very similar to the dipole case. The discussion at the end of § 3 anticipated this result. Configurations of Figure 1 that yield low PFs can significantly increase T_e compared to the dipole case and even compared to the nonmagnetic case; however, the observed strong pulsations, if really due to large surface temperature inhomogeneities, totally rule out such field configurations and thus such boundary conditions. From this we conclude that *the overall effect of the magnetic field on the star's effective temperature and its cooling is quite small and is well approximated by the dipole case*. Considering equation (6) with $\bar{\chi}^4 \ll 1$, and taking off another 5% for the quadrupole effect, we find that the reduction of T_e due to realistic field configuration is thus $\sim$0.8. The nonmagnetic T_b-T_e relationship is itself a decent first approximation to the dipolar one.

The cooling calculations of Page (1994), restricted to the photon-cooling era in which the T_b-T_e relationship is most important, were explicitly performed with the nonmagnetic case, in anticipation of the present results, and the conclusions therein about the necessity of extensive baryon pairing in the core of the Geminga neutron star are therefore still valid. For illustration, we show in Figure 7 several cooling curves with four boundary conditions from Figure 6, which show explicitly the smallness of the magnetic field's effects.

10. DISCUSSION AND CONCLUSIONS

10.1. *Modeling Pulsars' Surface Temperature Distribution*

We have completed our general study of thermal emission from magnetized neutron stars within the framework of blackbody emission. Our original intent was to determine whether the inhomogeneous surface temperature distribution induced by the anisotropy of heat flow in the envelope is strong enough to produce the pulsed fraction observed by *ROSAT* in Vela, Geminga, PSR 0656+14, and PSR 1055−52. We have shown explicitly in § 4 that most of the effect is in the geometric factor $\cos^{1/2}\Theta_B$ (eq. [4]), as presented originally by Greenstein & Hartke (1983), and fortunately the actual value of χ_0 (eq. [3]) is of little importance. Moreover, models of magnetized neutron star envelopes allow us to relate the interior temperature T_b to the maximum surface temperature $T_{s\parallel}$ quite reliably as long as the latter is higher than $\sim 3 \times 10^5$ K. The minimum surface temperature, $T_{s\perp}$, is poorly determined, but its actual value, equivalent to χ_0, is not really important. In short, *the surface temperature distribution of a magnetized neutron star can be modeled well enough for present practical purposes.*

Since we do not take into account the effect of the magnetic field on the emitted spectrum but only on the local surface temperature, our results are not sensitive to the actual strength of the field. As long as the magnetic field is stronger than a few times 10^{11} G, its effects saturate and we are mostly dealing with warm plates whose size is determined by the field orientation, Θ_B. When atmospheric effects are included, one can expect a real dependence on the field strength due to the presence of one or more absorption edges and a field-dependent anisotropy of the emission. As in the case of dipolar fields (Paper I), the composite BB spectrum produced by the temperature nonuniformity is close to that of a BB at the star's effective temperature, with some excess in the Wien tail (Fig. 3). The quadrupole-plus-dipole configurations that induce strong pulsations show an excess similar to the pure-dipole case, since they have warm and cold regions of similar areas, but many of the configurations that produce little pulsation yield a composite BB spectrum closer to a single-temperature BB spectrum since they have many warm regions and smaller cold regions.

10.2. *The Quadrupolar Component*

We showed in Paper I that dipolar surface fields do not allow one to reproduce the amplitude of the observed pulse profiles; however, we have shown here that the inclusion of a quadrupolar component is sufficient to raise the pulsed fraction up to or above the observed values. Gravitational lensing is crucial in this result, and the effect of the quadrupole, in the cases in which it does increase the pulsed fraction, is basically to push the two magnetic poles and the warm regions surrounding them closer to each other; the areas of the warm and cold regions do not change substantially compared to the pure-dipole case, but gravitational lensing is then less effective in keeping a warm region constantly in sight. This shift of the magnetic poles' location is in fact immediately seen in the cases of Geminga and PSR 1055−52, which are considered to be orthogonal rotators but show only a single wide peak in the soft X-ray band, while a dipolar field would produce two peaks (see also discussion in Halpern & Ruderman 1993). If we want to stick to a multipole description, strong octopolar components would make the matter worse, inducing still more warm regions and flattening the light curves even more. Thus the simple observation of significant pulsations implies that the surface field is dominated by the dipole with a significant quadrupolar component, but nevertheless weaker than the dipole, and that higher order components must be weaker.

It has been proposed that the presence of the quadrupole is also seen in the observed anomalous dispersion measure of the high-frequency versus low-frequency radio pulses that has been observed in several pulsars (Davies et al. 1984; Kuzmin 1992). *Similar observations of PSRs 0833−45, 0656+14, and 1055−52 would allow a direct comparison with the strengths of the quadrupoles needed for the interpretation of the radio and X-ray emission of these pulsars.* Failure to confirm the presence of a strong quadrupolar component could help constrain the size of these neutron stars through gravitational lensing. Another possibility is that the multipole expansion is inappropriate to describe the surface field (i.e., it would require the inclusion of many strong high-order components), as would be the case if the field has a sunspot-like structure; plate tectonics (Ruderman 1991a, 1991b, 1991c) does predict such a structure, which may be appropriate for cases like Geminga (Page et al. 1995).

Most dipole-plus-quadrupole configurations produce little observable pulsation, and it is surprising that all four observed pulsars have chosen an a priori highly improbable configuration that does increase PF. If we visualize the quadrupole as a pair of coplanar dipoles of equal strength but opposite direction, then the dipole-plus-quadrupole configurations that are successful in increasing PF are almost coplanar: there must be a good physical reason for this to happen in all four cases. The possible identification of a new young neutron star in a supernova remnant close to CTB 1 has recently been reported (Hailey & Craig 1996); this object appears to be similar in age and temperature to the Vela pulsar and also shows pulsations at a $10\% \pm 10\%$ level. If the detected X-rays are from the surface thermal emission and PF is above 10%, this would raise to five out of five the number of neutron stars in which a quadrupole with adequate orientation is present. The theory of plate tectonics (Ruderman 1991a, 1991b, 1991c) predicts that the crust of a young, fast-spinning pulsar should break under the stress produced by the internal superfluids and superconductors. Plate motion, toward the equator, will ensue, and the mutual attraction of the two magnetic poles may slowly pull them toward each other (as is apparently seen in Geminga and PSR 1055−52), inducing a strong quadrupolar component such as the one discovered in the present study.

The presence of such quadrupoles will have consequences for models of γ-ray emission near the polar caps, making it very difficult for photons to escape from this region of highly curved field lines. The influence of the displacement of the polar caps' position on the relative phases of the radio, X-ray, and γ-ray pulses also deserves study.

10.3. *Constraints on Neutron Star Size*

Within our present study, the observed pulsed fractions of Geminga and PSR 0656+14 cannot be reproduced if these stars have a radii of 7 km for a mass of 1.4 $M_\odot$ or, more generally, if their radii are of the order of $1.7R_S$, where R_S is the star's Schwarzschild radius. Moreover, a 10 km radius for a 1.4 $M_\odot$ star, i.e., $R = 2.4R_S$, can be "rejected at the 99% confidence level" in the sense that fewer than 10 models out of 1000 generated for Figure 1 can reproduce the observed PF for these same two neutron stars. Similarly, for Vela and PSR 1055−52, $R \sim 1.7R_S$ can be also be "rejected at the 99% confidence level" for the same reason, but $R = 2.4R_S$ is acceptable. Our results may thus favor rather large radii, above 10 km for a 1.4 $M_\odot$ mass, for all four neutron stars. These conclusions must be taken with extreme caution, for several reasons: (1) the dipole-plus-quadrupole description of the surface field may not be adequate, (2) anisotropic emission due to the magnetic field may significantly increase the observable pulsed fraction, (3) the emitted flux may be partially absorbed in the magnetosphere, and (4) the surface temperature may be controlled by factors other than heat flow from the hot interior. Each of these factors may, however, increase or reduce the observable pulsed fraction. We thus consider our results to be mostly illustrative but note that it is encouraging that the observed pulsed fractions fall within the range in which we could potentially rule out large classes of neutron star models through gravitational lensing of the surface thermal emission. We finally mention that gravitational lensing of the hot polar-cap emission may also provide complementary estimates of the neutron star radius: Yancopoulos, Hamilton, & Helfand (1994) found $R = (2.4 \pm 0.7)R_S$, or 10 ± 3 km at 1.4 $M_\odot$, for PSR 1929+10, but the anisotropy of emission and the lack of information on the location of the second polar cap make this estimate uncertain as well.

Interpretation of pulsar glitches as being due to a readjustment of the crustal neutron superfluid angular velocity also provides strong constraints on the neutron star size. For example, the analysis of Link, Epstein, & Van Riper (1992) of the Vela glitches also excludes very compact neutron stars in its "model independent" version and eliminates most of the present neutron star models in its "model dependent" version. However, glitches may be attributed to the core superfluids/superconductors (Sedrakian et al. 1995), in which case possible constraints on the neutron star size are much weaker. A third possibility, proposed recently but not yet studied, is the presence of a quark-bubble Coulomb lattice (Glendenning 1992) immersed in the nucleon-hyperon matter background of the core, in which pinning mechanisms may also be present; such models would also put only very weak constraints on the neutron/quark star sizes. In short, glitch models' constraints must be taken with caution, as must our results (see below), but both approaches seem to disfavor very small radii.

10.4. *Limitations of Blackbody Emission*

We have confirmed our previous result that, with BB emission, the observable pulsed fraction PF is unavoidably increasing with photon energy, at low energy, where the surface thermal emission is detected; we have also explained that this is due to the hardening of the BB spectrum with increasing temperature. The three pulsars Geminga, PSR 0656+14, and PSR 1055−52 show a decrease of PF with energy in the soft band, irreproducible with BB emission. The model of Page et al. (1995) produced such a decrease of PF by superposing two different spectra, a nonmagnetic hydrogen atmosphere at low temperature on most of the stellar surface and a magnetized hydrogen atmosphere on two warm magnetized plates: the warm, magnetic spectrum is much softer than the cold, nonmagnetic one, and PF decreases strongly with energy. Extrapolating from this result, we may speculate that the decrease of PF with energy is due to the warmest regions' emitting a softer spectrum than the neighboring colder regions, softening that should be induced by differences in magnetic field strength and/or orientation. We also showed in § 8 that the separation of the soft thermal component and the hard tail is large enough to make the contribution of the latter in the soft band quite small: the observed decrease of PF is an intrinsic feature of the surface thermal emission and not due to an interference of these two components as proposed by Halpern & Ruderman (1993) in the case of Geminga.

These limitations of BB emission may cast doubts on the validity of our results. As we stated in § 1, we consider that modeling neutron stars' thermal emission with BB emission is a mandatory first step, and our study does allow us to delimitate more clearly the limitations of this approach. A BB model is certainly not adequate for reliable estimates of pulsars' surface temperature, as well as size and distance, from spectral fits (see, e.g., Ögelman et al. 1993). However, modeling of the pulse profiles is probably less dependent on the exact atmospheric characteristics since the anisotropy of the emission from the atmosphere is not very strong at low energy, and it is unlikely to affect dramatically our conclusions on the effect of gravitational lensing and neutron star sizes. Our results obviously have to be taken only as a first step that we hope can indicate the direction to be taken for future work.

10.5. *Neutron Star Cooling*

We have finally applied our model to assess the effect of the crustal magnetic field on the outer boundary condition used in neutron star cooling models. We have shown that the global effect of the magnetic field, compared to the nonmagnetic case, is very small and consists of a slight reduction (at low field) or slight increase (at high field) of the heat flux in the envelope, which results in a slightly lower (higher) effective temperature T_e for a given inner temperature T_b. This is in sharp distinction to the case in which magnetic effects are naively applied under the assumption of a uniformly magnetized surface, implying a significant increase of T_e as compared to the nonmagnetic case.

After our completion of the present work, Shibanov & Yakovlev (1996) presented models of magnetized neutron star cooling with a dipolar surface magnetic field along the same lines as presented here.[1] They reached basically the same conclusions as we do but found larger effects, probably due to the fact that they used the envelope models of Van Riper (1988) while we followed Hernquist (1985), whose models are different at low temperatures. However, we mentioned in Paper I that envelope models at $T_e < 3 \times 10^5$ K are not reliable, so the differences should not be taken too seriously. Nevertheless, the discrepancies between Shibanov & Yakovlev's work and ours outline the necessity of better models of magnetized envelopes for more accurate applications to cooling.

10.6. *Warning about the Relevance of the Model*

Finally, we repeat the warning expressed in Paper I about the relevance of our study: strong heating of the surface by magnetospheric hard X-rays and/or substantial magnetospheric absorption of the emitted flux, as proposed by Halpern & Ruderman (1993), could seriously invalidate our results (Page 1995b). The possible detection of pulsed γ-rays from PSR 0656+14 (Ramanamurthy et al. 1996) would mean that all four pulsars we study are copious γ-ray emitters, and heating of the neutron star surface by such energetic magnetospheres is not an unreasonable hypothesis. In the original Halpern & Ruderman (1993) model for

[1] These authors misinterpreted our writing of eqs. (6) and (7) in Paper I, because of our abbreviated notation, and mentioned a correction to them. The same two equations were written more explicitly here (eqs. [2] and [3]) to show that our method and theirs are identical.

Geminga, the flow of electrons/positrons onto the polar caps produced a luminosity $L_p \sim 2.6 \times 10^{32}$ ergs s^{-1}, radiated away as hard X-rays, which would then be backscattered onto the neutron star's surface and reemitted as soft surface thermal X-rays. The X-ray luminosity of Geminga is $\sim 2 \times 10^{31}$ ergs s^{-1} for the soft thermal component and 8×10^{29} ergs s^{-1} for the hard tail (for a distance of 160 pc, as measured by Caraveo et al. 1996), so even a small proportion of the hard polar X-rays hitting back upon the surface could explain the observed temperature. This model however had two problems. The first is that the *total* predicted X-ray luminosity was more than 1 order of magnitude higher than observed. The argument has been recently revised and the polar-cap luminosity scaled down by Zhu & Ruderman (1996), who now obtain $L_p \sim 8 \times 10^{30}$ ergs s^{-1}. This is much closer to what is observed and may be the factor controlling Geminga's surface temperature. However, the second problem remains, namely, that the observed soft thermal X-ray flux is ~ 30 times larger than the hard flux, so that in this model almost all the polar-cap hard X-rays must be scattered back onto the stellar surface. On the other hand, neutron star cooling models are also perfectly able to explain the observed temperature (Page 1994). We can only hope that future work will elucidate this dilemma.

We are grateful to Yu. A. Shibanov for many discussions. This work was supported by a UNAM-DGAPA grant (IN105794, continued through grant IN105495). D. P. acknowledges support from a *Cátedra Patrimonial* of CONACyT.

APPENDIX

THE QUADRUPOLAR COMPONENTS AND GRAVITY EFFECTS

We write the quadrupolar component of the magnetic field as

$$\boldsymbol{B}^Q = \sum_{i=0}^{4} Q_i \left(\frac{R}{r}\right)^4 \boldsymbol{b}_i, \tag{A1}$$

where the five generating fields $\boldsymbol{b}_i$ are listed in Table 1. Considering the generating quadrupolar components separately at the star's surface, one finds that all components reach a maximum strength of 1 and that $\boldsymbol{b}_0$ has a minimum of $1/\sqrt{5}$ $(=0.45)$ while the other four have a minimum of zero. They have four magnetic poles, except for $\boldsymbol{b}_0$, whose "south" pole is degenerate and becomes a line covering the whole equator. However, the general quadrupolar field $\boldsymbol{B}^Q$ can have up to six poles, south and north poles always being in an even number. When the quadrupole is added to a dipole, we can have again up to six poles, and the number of north (south) poles can be odd. Note finally that the scale value of the dipolar component we use is the field strength at a magnetic pole, i.e., twice the value commonly considered, so that all field scales we cite always refer to the maximum field strength of the cited component at the stellar surface in flat spacetime.

We also include the effect of gravity on the magnetic field. It can be written in the form of four multiplicative factors, two for the radial component of the magnetic field and two for its angular components: if B_r, B_τ ($\tau = \theta$ or ϕ) denote the radial and angular components of the magnetic field in the absence of a gravitational field, then

$$B^D_{r,g} = f_1 B^D_r\,, \qquad B^D_{\tau,g} = \sqrt{g_{00}}\, g_1 B^D_\tau \tag{A2}$$

yield the dipolar fields in the presence of a gravitational field, and

$$B^Q_{r,g} = f_2 B^Q_r\,, \qquad B^Q_{\tau,g} = \sqrt{g_{00}}\, g_2 B^Q_\tau \tag{A3}$$

yield the quadrupolar fields in the same situation. The factors in the previous equalities are

$$f_1 = -\frac{3}{x^3}\left[\ln(1-x) + \frac{1}{2}x(x+2)\right], \qquad g_1 = -2f_1 + \frac{3}{1-x}, \tag{A4}$$

$$f_2 = \frac{10}{3x^4}\left[6\ln(1-x)\,\frac{(3x-4)}{x} + x^2 + 6x - 24\right], \qquad g_2 = \frac{10}{x^4}\left[6\ln(1-x)\,\frac{2-x}{x} + \frac{x^2-12x+12}{1-x}\right], \tag{A5}$$

where $x = R_S/r$, with $R_S = 2GM/c^2$ being the star's Schwarzschild radius, and $g_{00} = 1 - x$ is the time component of the metric (Muslimov & Tsygan 1987). These corrections of course tend toward unity at large distances. The values of f_l and g_l at the

TABLE 1

SPHERICAL COMPONENTS OF THE FIVE GENERATING QUADRUPOLAR FIELDS AND LOCATION OF THE MAGNETIC POLES

	$\boldsymbol{b}_0$	$\boldsymbol{b}_1$	$\boldsymbol{b}_2$	$\boldsymbol{b}_3$	$\boldsymbol{b}_4$
b_r	$(3/2)\cos^2\theta - 1$	$\sin 2\theta \sin\phi$	$-\sin 2\theta \cos\phi$	$-\sin^2\theta \sin 2\phi$	$\sin^2\theta \cos 2\phi$
b_θ	$\frac{1}{2}\sin 2\theta$	$-\frac{2}{3}\cos 2\theta \sin\phi$	$\frac{2}{3}\cos 2\theta \cos\phi$	$\frac{1}{3}\sin 2\theta \sin 2\phi$	$-\frac{1}{3}\sin 2\theta \cos 2\phi$
b_ϕ	0	$-\frac{2}{3}\cos\theta \cos\phi$	$-\frac{2}{3}\cos\theta \sin\phi$	$\frac{2}{3}\sin\theta \cos 2\phi$	$\frac{2}{3}\sin\theta \sin 2\phi$
Poles:					
"North"	$\theta = 0, \pi$	$(\theta, \phi) = \begin{cases}(\pi/4, \pi/2)\\(3\pi/4, 3\pi/2)\end{cases}$	$(\theta, \phi) = \begin{cases}(\pi/4, \pi)\\(3\pi/4, 0)\end{cases}$	$(\theta, \phi) = \begin{cases}(\pi/2, 3\pi/4)\\(\pi/2, 7\pi/4)\end{cases}$	$(\theta, \phi) = \begin{cases}(\pi/2, 0)\\(\pi/2, \pi)\end{cases}$
"South"	$\theta = \frac{\pi}{2}$	$(\theta, \phi) = \begin{cases}(\pi/4, 3\pi/2)\\(3\pi/4, \pi/2)\end{cases}$	$(\theta, \phi) = \begin{cases}(\pi/4, 0)\\(3\pi/4, \pi)\end{cases}$	$(\theta, \phi) = \begin{cases}(\pi/2, \pi/4)\\(\pi/2, 5\pi/4)\end{cases}$	$(\theta, \phi) = \begin{cases}(\pi/2, \pi/2)\\(\pi/2, 3\pi/2)\end{cases}$

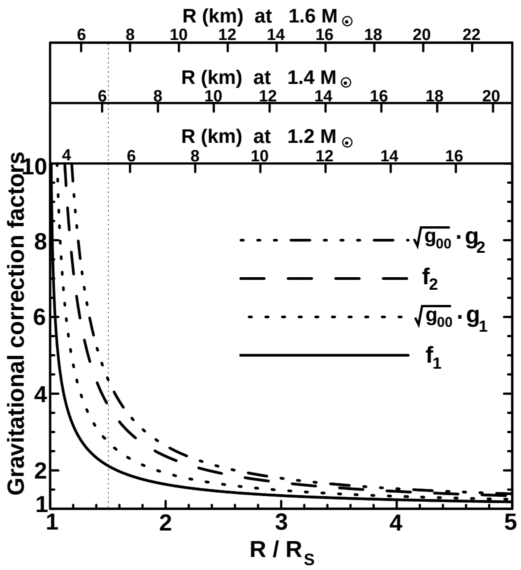

FIG. 8.—Gravitational correction factors for the radial (r), f_l, and spherical (θ, ϕ), g_l, parts of the dipolar ($l = 1$) and quadrupolar ($l = 2$) components of the magnetic field at the stellar surface as a function of the ratio of the star's radius R to its Schwarzschild radius R_S or of the actual star's radius at masses of 1.2, 1.4, and 1.6 $M_\odot$.

stellar surface, i.e., at $x = R_S/R$, are plotted in Figure 8; the effect is stronger on the quadrupole than on the dipole, simply because of the stronger r-dependence of the former. If $R \to R_S$, then f_l and g_l tend to ∞, which means that, for a given surface field, the field "at infinity" vanishes; this is a particular case of the "no hair" theorem for nonrotating black holes (see, e.g., Misner, Thorne, & Wheeler 1973).

REFERENCES

Ainsworth, T. L., Wambach, J., & Pines, D. 1989, Phys. Lett. B, 222, 173
Caraveo, P. A., Bignami, G. F., Mignani, R., & Taff, L. G. 1996, ApJ, 461, L91
Davies, J. G., Lyne, A. G., Graham-Smith, F., Izvekova, V. A., Kuzmin, A. D., & Shitov, Yu. P. 1984, MNRAS, 211, 57
Finley, J. P., Ögelman, H., & Kiziloğlu, Ü. 1992, ApJ, 394, L21
Friedman, B., & Pandharipande, V. R. 1981, Nucl. Phys. A, 361, 502
Glendenning, N. K. 1992, Phys. Rev. D, 46, 1274
Greenstein, G., & Hartke, G. J. 1983, ApJ, 271, 283
Hailey, C. J., & Craig, W. W. 1996, ApJ, 455, L151
Halpern, J. P., & Holt, S. S. 1992, Nature, 357, 222
Halpern, J. P., & Ruderman, M. 1993, ApJ, 415, 286
Haensel, P., & Gnedin, O. 1994, A&A, 290 458
Hernquist, L. 1985, MNRAS, 213, 313
Hoffberg, M., Glassgold, A. E., Richardson, R. W., & Ruderman, M. 1970, Phys. Rev. Lett., 24, 775
Kuzmin, A. D. 1992, in IAU Colloq. 128, The Magnetospheric Structure and Emission Mechanisms of Radio Pulsars, ed. T. H. Hankins, J. M. Rankin, & J. A. Gil (Zielona Góra, Poland: Pedagogical Univ. Press), 2
Link, B., Epstein, R. I., & Van Riper, K. A. 1992, Nature, 359, 616
Lyne, A. G., & Manchester, R. N. 1988, MNRAS, 234, 477
Misner, C. W., Thorne, K. S., & Wheeler, J. H. 1973, Gravitation (San Francisco: W. H. Freeman)
Muslimov, A. G., & Tsygan, A. I. 1987, Soviet Astron., 30, 567
Ögelman, H. 1995, in The Lives of the Neutron Stars, ed. A. Alpar, Ü. Kiziloğlu, & J. van Paradijs (NATO ASI Ser. C, 450) (Dordrecht: Kluwer), 101
Ögelman, H., & Finley, J. P. 1993, ApJ, 413, L31
Ögelman, H., Finley, J. P., & Zimmermann, H.-U. 1993, Nature, 361, 136
Page, D. 1994, ApJ, 428, 250
———. 1995a, ApJ, 442, 273 (Paper I)
———. 1995b, Space Sci. Rev., 75, 437
Page, D., & Sarmiento, A. 1996, in Röntgenstrahlung from the Universe, ed. H.-U. Zimmermann, J. Trümper, & H. W. Yorke (MPE Rep. 263) (Garching: MPE), 171 (astro-ph/9601175)
Page, D., Shibanov, Yu. A., & Zavlin, V. E. 1995, ApJ, 451, L21
Pavlov, G. G., Shibanov, Yu. A., Ventura, J., & Zavlin, V. E. 1994, A&A, 289, 837
Possenti, A., Mereghetti, S., & Colpi, M. 1996, A&A, 313, 565
Ramanamurthy, P. V., Fichtel, C. E., Kniffen, D. A., Sreekumar, P., & Thompson, D. J. 1996, ApJ, 458, 755
Ruderman, M. 1991a, ApJ, 366, 261
———. 1991b, ApJ, 382, 576
———. 1991c, ApJ, 382, 587
Sedrakian, A. D., Sedrakian, D. M., Cordes, J. M., & Terzian, Y. 1995, ApJ, 447, 324
Shibanov, Yu. A., & Yakovlev, D. G. 1996, A&A, 309, 171
Van Riper, K. A. 1988, ApJ, 329, 339
———. 1991, ApJS, 75, 449
Yancopoulos, S., Hamilton, T. T., & Helfand, D. J. 1994, ApJ, 429, 832
Zavlin, V. E., Pavlov, G. G., Shibanov, Yu. A., & Ventura, J. 1995, A&A, 297, 441
Zhu, T., & Ruderman, M. 1996, ApJ, submitted